

QuantileMark: A Message-Symmetric Multi-bit Watermark for LLMs

Anonymous ACL submission

Abstract

As large language models become standard backends for content generation, practical provenance increasingly requires multi-bit watermarking. In provider-internal deployments, a key requirement is message symmetry: the message itself should not systematically affect either text quality or verification outcomes. Vocabulary-partition watermarks can break message symmetry in low-entropy decoding: some messages are assigned most of the probability mass, while others are forced to use tail tokens. This makes embedding quality and message decoding accuracy message-dependent. We propose QuantileMark, a white-box multi-bit watermark that embeds messages within the continuous cumulative probability interval $[0, 1)$. At each step, QuantileMark partitions this interval into M equal-mass bins and samples strictly from the bin assigned to the target symbol, ensuring a fixed $1/M$ probability budget regardless of context entropy. For detection, the verifier reconstructs the same partition under teacher forcing, computes posteriors over latent bins, and aggregates evidence for verification. We prove message-unbiasedness, a property ensuring that the base distribution is recovered when averaging over messages. This provides a theoretical foundation for generation-side symmetry, while the equal-mass design additionally promotes uniform evidence strength across messages on the detection side. Empirical results on C4 continuation and LFQA show improved multi-bit recovery and detection robustness over strong baselines, with negligible impact on generation quality.

1 Introduction

Large language models (LLMs) have become standard backends for applications ranging from dialogue assistance and content creation to code generation and data analysis (OpenAI, 2022). As high-quality synthetic text becomes ubiquitous and inexpensive, provenance has emerged as a practical ne-

cessity: platforms and providers must attribute the origin of content and its deployment settings. This capability is critical not only for mitigating misinformation but also for policy enforcement, abuse response (e.g., toxic content), copyright disputes, and enterprise compliance (Yang et al., 2025). A common attribution scenario is *internal* to the provider, where the entity hosting the model also controls and provides the detection service (e.g., via a verification API).

Generative watermarking addresses this need by embedding a covert signal during the decoding process, enabling a detector to verify the model’s authorship (Kirchenbauer et al., 2023). While early work focused on *zero-bit* schemes for binary presence detection, real-world deployments increasingly demand *multi-bit* provenance to encode metadata such as user IDs, model versions, or timestamps (Yoo et al., 2024). We represent the provenance message as a binary string segmented into m -bit symbols, so each symbol takes one of $M = 2^m$ discrete values. At each watermarking step, we embed one symbol and can convey up to m bits of information. For example, a 24-bit message can be encoded as 12 symbols when $m = 2$.

Unlike zero-bit watermarking, where the detector only answers a binary question of presence, multi-bit provenance requires decoding a specific message (e.g., a user ID). This distinction introduces a critical requirement: **message symmetry**. Message symmetry means that the message itself should not systematically affect either text quality or verification outcomes. In particular, this concern arises in two places. During generation, messages should receive comparable probability-mass budgets so that text quality does not depend on the identifier. During detection, evidence should accumulate comparably across messages so that watermark detection are not message-dependent. Ensuring this symmetry is essential for operational fairness, as it guarantees that the provider can deliver consistent

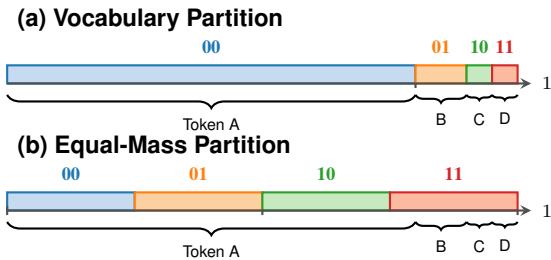


Figure 1: Impact of probability mass partitioning strategies on message symmetry under a low-entropy distribution. (a) Vocabulary Partition allocates uneven probability budgets to messages that should ideally be weighted equally. (b) Equal-Mass Partition assigns a fixed probability budget to each message.

service quality and attribution reliability across the entire user base.

Existing generative watermarks can be broadly grouped into *distortionary* and *distribution-preserving* designs. Both design lines face challenges when message symmetry is required for multi-bit provenance.

Distortionary schemes typically employ a **vocabulary partition** to construct the signal (Yoo et al., 2024). For a message space of size M , these methods partition the vocabulary into M disjoint sets and apply a logit bias to the subset corresponding to the target symbol. This approach, however, introduces severe asymmetry under low-entropy decoding. Consider a step where the model assigns probabilities $\{0.8, 0.1, 0.05, 0.05\}$ to its top candidates, as shown in Figure 1. If the token with probability 0.8 falls into the partition set for one value, embedding that value is almost free: the model outputs its preferred token and the detector observes the signal with high probability. Conversely, for the other $M - 1$ values, their assigned sets may contain only low-probability tail tokens. Embedding these values forces the model to override its natural choice, which degrades text quality while simultaneously yielding weaker statistical evidence. Consequently, the expected evidence averaged over all messages is diluted.

Distribution-preserving methods ensure the watermarked output preserves the base distribution when marginalized over randomness. This goal can already mitigate message-dependent distortion on the generation side. However, constrained by the requirement of **black-box verification**, these schemes typically prioritize stealth through *minimal stepwise distortion* (Jiang et al., 2025). This creates a fundamental bottleneck for multi-bit

provenance: the evidence is often too subtle for robust message recovery. In provider-internal settings with white-box access, such constraints are unnecessary. A more attractive direction is to enforce message symmetry explicitly, then exploit its benefit: allocate each symbol a fixed probability budget and permit larger, controlled deviations, ensuring effective evidence accumulation.

To overcome the structural asymmetry of vocabulary partitioning and the evidence limitations of existing distribution-preserving designs, we introduce **QuantileMark**, a white-box multi-bit watermark based on continuous probability mass partitioning. At each step, QuantileMark partitions the cumulative probability interval $[0, 1)$ into M bins of equal probability mass and encodes a symbol by sampling within the corresponding bin (Figure 2). During detection, the verifier reconstructs the same partition to compute posteriors for the latent bins. Equal-mass allocation enforces message symmetry by construction, and it turns symmetry into stronger and more stable stepwise evidence regardless of context entropy.

In summary, our contributions are threefold. First, we introduce QuantileMark, a provenance framework that guarantees a uniform probability budget for every message symbol via quantile partitioning, accompanied by a white-box detector that computes posteriors for decoding. Second, we formalize the notion of message-unbiasedness and prove that QuantileMark satisfies this property, providing a theoretical guarantee for generation-side symmetry. Finally, we demonstrate that QuantileMark outperforms vocabulary-based baselines on C4 and LFQA in recovery and robustness, while maintaining generation quality¹.

2 Preliminaries

We study a provider-internal watermarking setting where a model generates a sequence $x_{1:T}$ using a fixed secret key K . Let $h_t := x_{<t}$ denote the history at step t , and let $p_0(\cdot | h_t)$ denote the base next-token distribution. Our goal is to embed a message $S = (s_1, \dots, s_H)$ consisting of H discrete symbols. Each symbol s_h encodes m bits of information and is drawn from the set $[M] := \{0, \dots, M - 1\}$, where $M = 2^m$.

Position Allocation. Unlike zero-bit presence detection, recovering a multi-bit message requires locating where each symbol is embedded. A stan-

¹Our code will be released soon.

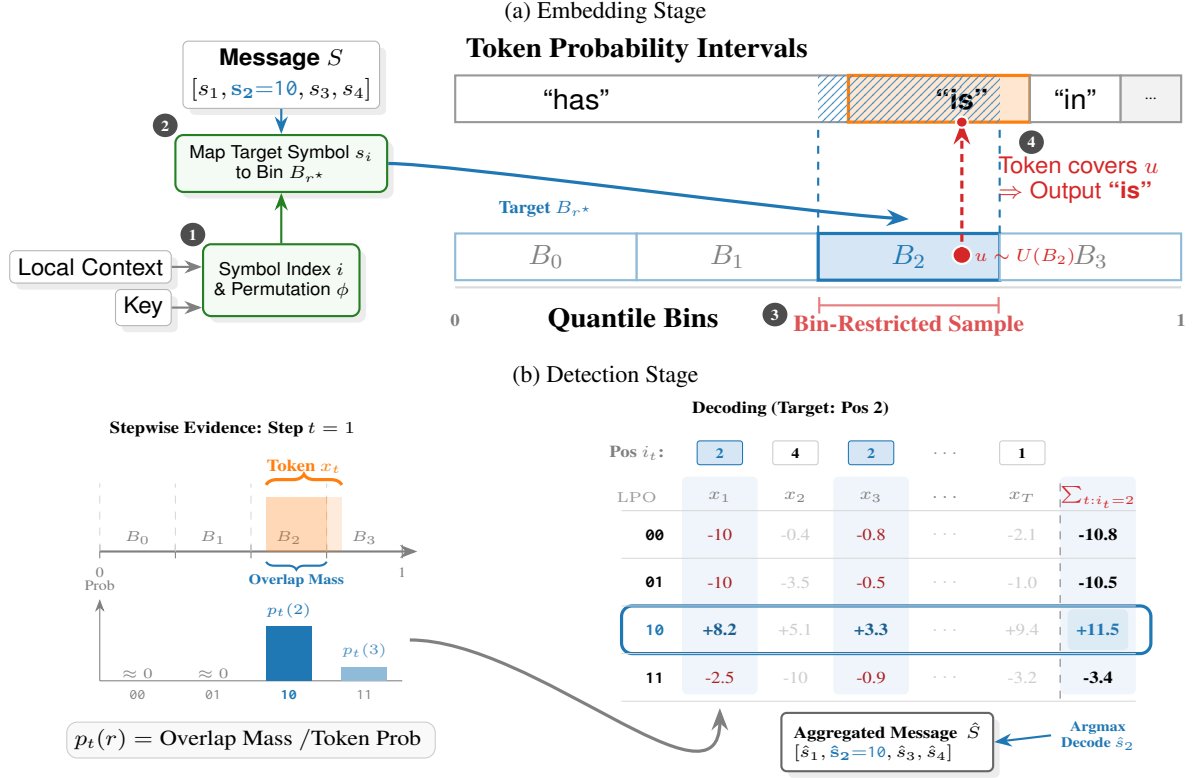


Figure 2: Overview of QuantileMark, where $m = 2, H = 4$. (a) **Embedding**: The key-derived logic (green) maps symbol to target bin B_{r^*} (blue frame). A pivot u (red dashed line) is sampled uniformly within this bin, forcing the selection of the token is whose interval covers u . (b) **Detection**: Posteriors (blue bars) form the evidence LPO at this step. These scores are aggregated across steps assigned to position $i_t = 2$ (right, blue columns) to decode \hat{s}_2 .

standard abstraction is *position allocation* (Yoo et al., 2024): a keyed function maps each step t to an index $i_t \in \{1, \dots, H\}$. This implies that step t carries evidence *only* about the specific message symbol s_{i_t} .

Vocabulary Partitioning as Multi-Bit Channel. Many existing methods construct the channel by partitioning the vocabulary. At step t , the vocabulary is split into M disjoint sets $\{\mathcal{V}_t^{(r)}\}_{r=0}^{M-1}$. To embed symbol s_{i_t} , the sampler promotes tokens in $\mathcal{V}_t^{(s_{i_t})}$. In this paradigm, the abstract message symbol is tied directly to discrete token identities.

CDF and Quantile Function View of Sampling. It is convenient to represent discrete sampling using the cumulative distribution function (CDF) F and its inverse, the **quantile function** $Q(u) = F^{-1}(u)$. Under an ordering of tokens at step t , each token corresponds to a specific interval on the **cumulative probability interval** $[0, 1)$ whose length equals its probability. Standard sampling is operationally equivalent to drawing $u \sim \text{Unif}[0, 1)$ and selecting the output token via

$x = Q(u)$, which returns the token whose interval contains u . This geometric view allows us to decouple the channel from discrete token identities by defining the watermark logic directly on the continuous domain of the quantile function. We refer to embedding strategies that operate on this continuous interval as **quantile watermarking**.

3 Methodology: Equal-Mass Quantile Watermarking

We propose **QuantileMark**, a white-box watermarking framework designed to ensure **message symmetry** by defining the embedding channel on the cumulative probability interval rather than vocabulary space.

The framework consists of two procedures (Figure 2). During generation, QuantileMark partitions the stepwise cumulative probability interval into M equal-mass quantile bins and samples a token strictly from the bin assigned to the target message symbol. During detection, the verifier reconstructs this quantile geometry, computing the posterior

probability of the latent bin to aggregate evidence and decode the message.

3.1 Setup: Message and Position Allocation

Let $x_{1:T}$ be the generated sequence and h_t the history at step t . We embed a message $S = (s_1, \dots, s_H)$ consisting of H symbols, where each symbol $s_h \in \{0, \dots, M-1\}$ and $M = 2^m$.

At each step t , we derive pseudo-random parameters from a secret key K and a local context window g_t (the previous w tokens). Specifically, we generate a position allocation index $i_t \in \{1, \dots, H\}$ that determines which message symbol s_{i_t} to embed at the current step, alongside a keyed permutation ϕ_t that maps this symbol to a specific target bin index on the CDF.

The permutation ϕ_t ensures that a fixed symbol value is not systematically bound to the same quantile bins, which is essential for the unbiasedness statements in Section 3.4.

3.2 Embedding via Quantile Partitioning

The core of our embedding strategy is to enforce a uniform probability budget for every symbol by operating on the continuous domain of the quantile function. This requires partitioning the unit interval and calculating the mass overlap to bridge the continuous design with the discrete vocabulary.

Quantile Geometry and Overlap Mass. At step t , we sort the vocabulary by probability to map each token v to a sub-interval $I_t(v) \subset [0, 1]$ of length $p_0(v|h_t)$. We simultaneously partition $[0, 1]$ into M fixed bins $B_r = [r/M, (r+1)/M)$. The alignment between token intervals and bins is captured by the **overlap mass**:

$$\mu_t(v, r) = |I_t(v) \cap B_r|. \quad (1)$$

This explicitly quantifies the mass of v falling within B_r , bridging the continuous design with the discrete vocabulary and enabling the use of partial mass from tokens that straddle bin boundaries.

Bin-Restricted Sampling. To embed the target symbol s_{i_t} , we identify the target bin $r_t^* = \phi_t(s_{i_t})$. Instead of standard sampling (drawing $u \in [0, 1]$ globally), QuantileMark samples a random pivot u_t strictly within the target bin $B_{r_t^*}$. The output token x_t is determined by finding the token whose interval $I_t(x_t)$ contains u_t . The resulting watermarked distribution for a chosen bin r is:

$$p_{\text{wm}}(v | h_t, r) = M \cdot \mu_t(v, r). \quad (2)$$

This sampling mechanism guarantees that every target symbol receives an identical probability budget ($1/M$) regardless of context entropy. Consequently, this structurally enforces message symmetry while effectively exploiting it: in contrast to minimal-distortion baselines like StealthInk, we concentrate the entire probability mass into the target bin, substantially boosting the stepwise evidence available for detection.

3.3 Decoding and Detection

The detection process follows a *decode-then-test* paradigm: we first reconstruct the latent quantile geometry to recover the most likely message \hat{S} , and then compute a detection score based on the confidence of this recovery.

Stepwise Evidence Extraction. The core of our detection strategy is to recover soft evidence about the embedding channel using teacher forcing. At each step t , the detector reconstructs the base distribution $p_0(\cdot | h_t)$ and the quantile geometry. The observed token x_t occupies the interval $I_t(x_t)$. Given that the sampling pivot must lie within this interval, the posterior probability that it originated from bin r is the proportion of the token’s mass overlapping that bin:

$$p_t(r) = P(R_t = r | x_t, h_t) = \frac{\mu_t(x_t, r)}{p_0(x_t | h_t)}. \quad (3)$$

Crucially, this posterior provides soft evidence. Unlike vocabulary partitioning, which forces a hard assignment (casting a vote for a single symbol and rejecting the other $M-1$), $p_t(r)$ distributes support proportional to the overlap mass. For example, a token straddling bins r_1 and r_2 yields positive support for both while decisively ruling out non-overlapping bins.

To aggregate this evidence numerically, we compute the Log Posterior Odds (LPO):

$$\text{LPO}_t(r) = \log \left(\frac{p_t(r)}{1 - p_t(r)} \right). \quad (4)$$

For numerical stability, we clip $p_t(r)$ to the range $[\epsilon, 1 - \epsilon]$.

Message Decoding. Since the position allocation i_t is deterministic given the key, we aggregate evidence for each message symbol s_h independently. The decoder identifies the symbol \hat{s}_h that maximizes the cumulative LPO across all steps assigned to index h :

$$\hat{s}_h = \arg \max_{s \in \{0, \dots, M-1\}} \sum_{t:i_t=h} \text{LPO}_t(\phi_t(s)). \quad (5)$$

Here, $\phi_t(s)$ maps the candidate symbol s to its corresponding bin index at step t .

Sequence-Level Scoring. Once the message $\hat{S} = (\hat{s}_1, \dots, \hat{s}_H)$ is decoded, we evaluate the overall presence of the watermark. We define the implied target bin path as $\hat{r}_t = \phi_t(\hat{s}_{i_t})$ and compute the average evidence along this path: $T(x_{1:T}) = \frac{1}{T} \sum_{t=1}^T \text{LPO}_t(\hat{r}_t)$

The watermark is detected if $T(x_{1:T}) > \theta$, where θ is a threshold calibrated to control the false positive rate on non-watermarked text.

3.4 Unbiasedness Properties of Equal-Mass Channelization

We assume a uniform prior over the message space. Under this assumption, the target symbol s at any given step is uniformly distributed over $[M]$.

Definition 1 (Message-unbiasedness at a step). Fix a context h_t and key K . Let s be a target symbol drawn uniformly from $[M]$, and let $R = \phi_t(s)$ be the relabeled bin index. The scheme is message-unbiased if, for all tokens v ,

$$\mathbb{E}_s [p_{\text{wm}}(v | h_t, R)] = p_0(v | h_t).$$

Lemma 1 (Equal-mass bins imply message-unbiasedness). Assume ϕ_t maps a uniform symbol to a uniform bin in $[M]$, then QuantileMark is message-unbiased at step t .

The proof follows from the linearity of expectation and the partition of unity property of the quantile bins; see Appendix A.2 for details.

Message-unbiasedness ensures that, on average, the watermark introduces no distortion if the message is unknown. Crucially, this property serves as a structural pathway to satisfying the dual notion of **cipher-unbiasedness** (Jiang et al., 2025), which requires the distribution to be preserved when the message is fixed but the key is randomized.

Definition 2 (Cipher-unbiasedness at a step). Fix a context h_t , a key K , and a symbol $s \in [M]$. Let Z be a seed random variable, and let $\Phi_{t,Z}$ denote the resulting key-conditioned permutation on $[M]$ produced from Z . The scheme is cipher-unbiased if, for all tokens v ,

$$\mathbb{E}_Z [p_{\text{wm}}(v | h_t, \Phi_{t,Z}(s))] = p_0(v | h_t).$$

QuantileMark satisfies Definition 2 whenever, for any fixed s , the induced bin index $\Phi_{t,Z}(s)$ is uniform on $[M]$ under the seed distribution. The proof is given in Appendix A (Lemma 3).

4 Experiments

We evaluate QuantileMark in a provider-internal setting, focusing on accurate *multi-bit* recovery from clean generations and robustness against realistic deployment mismatches. Our results confirm that QuantileMark significantly improves detection stability over vocabulary-based baselines while maintaining generation quality.

4.1 Experimental Setup

We conduct experiments on two tasks: open-ended continuation on C4 (Raffel et al., 2020) using Llama-2-7B (Touvron et al., 2023), and long-form QA on ELI5/LFQA (Fan et al., 2019) using Llama-3.1-8B-Instruct (Grattafiori et al., 2024). We pair each task with a suitable model, using a base model for continuation and an instruction-tuned model for QA, to ensure the evaluation reflects realistic deployment behavior. Unless otherwise stated, results are averaged over 500 watermarked and 500 non-watermarked samples per task, all fixed to a length of $T = 300$ tokens. We use human references as non-watermarked text to simulate realistic detection against organic text. Appendix E.1 additionally evaluates against non-watermarked model generations to isolate the watermark signal from distributional mismatch.

We embed a 24-bit message using top- $k=128$ sampling and temperature $\tau=1.0$. We compare QuantileMark ($m=2$) against MPAC (Yoo et al., 2024) ($m=2, \gamma=0.25, \delta=2.0$) and StealthInk (Jiang et al., 2025) ($m=1$), following the recommended settings for best trade-offs. Detection of QuantileMark reconstructs geometry via teacher forcing on output tokens (adding chat template headers for Instruct models) with matching top- k/τ ; detector mismatch is analyzed separately in Section 4.4. We report Bit Acc (bit-wise accuracy, averaged over 500 watermarked samples), detection AUC, TPR@1%FPR, and perplexity (PPL).

4.2 Generation and Detection Results

Table 1 summarizes the generation and detection performance of different methods on two tasks. QuantileMark achieves consistently strong multi-bit recovery and near-saturated detection, with high bit accuracy and AUC and TPR@1%FPR close to 1.0 on both C4 and LFQA. Notably, these gains persist on LFQA, where the next-token distribution is often more peaked and vocabulary-partition methods can allocate highly uneven probability mass

Method	C4					LFQA				
	Bit Acc \uparrow	AUC \uparrow	TPR@1%FPR \uparrow	PPL \downarrow	Time (s) \downarrow	Bit Acc \uparrow	AUC \uparrow	TPR@1%FPR \uparrow	PPL \downarrow	Time (s) \downarrow
No watermark	–	–	–	7.684	–	–	–	–	2.647	–
MPAC	0.9702	0.9887	0.9800	10.351	0.103	0.8770	0.9756	0.8056	3.793	0.111
StealthInk	0.9003	0.9869	0.7920	8.235	0.645	0.7447	0.8301	0.2425	2.636	1.013
QuantileMark (ours)	0.9893	0.9995	0.9840	7.404	0.343	0.9500	0.9997	1.0	2.759	0.348

Table 1: Generation and detection performance on C4 and LFQA with 24 bits embedded in 300 tokens. Time (s) denotes average detection time per sample.

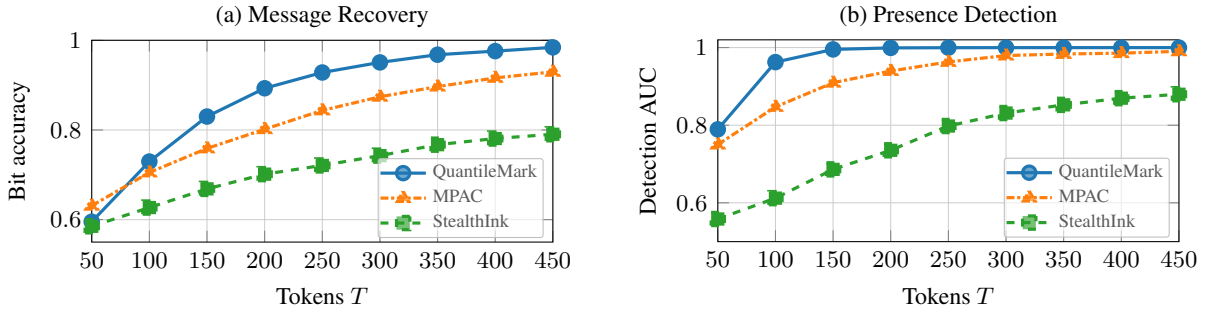


Figure 3: Varying detection length T on Llama-3.1-8B-Instruct for LFQA.

across symbol values, destabilizing detection.

In terms of generation quality, QuantileMark maintains PPL close to the unwatermarked baseline; minor fluctuations (e.g., 7.404 vs 7.684 on C4) fall within expected finite-sample randomness, consistent with our theoretical message-unbiasedness. In contrast, MPAC incurs a noticeable PPL increase due to distortionary green-list bias, while StealthInk shows weaker recovery at the same message length. This performance comes with negligible operational overhead: although detection requires a model forward pass, the computational cost is strictly bounded by the generation latency itself, making verification inherently affordable for any provider capable of hosting the service.

Varying the generated length T (Figure 3) confirms that QuantileMark accumulates evidence efficiently, reaching high recovery and detection rates with fewer tokens than baselines.

We next vary the symbol size m while keeping the message length fixed at 24 bits. Figure 4 shows a trade-off between symbol resolution and reliable evidence. Moderate choices ($m = 2, 3$) perform best, while $m = 4$ sharply reduces recovery even though detection remains strong. Intuitively, since a single observed token reveals limited information about the latent bin (Appendix A.3), increasing m under a fixed-length budget fails to provide sufficient supporting tokens for M -ary decisions. This effectively dilutes the information per sym-

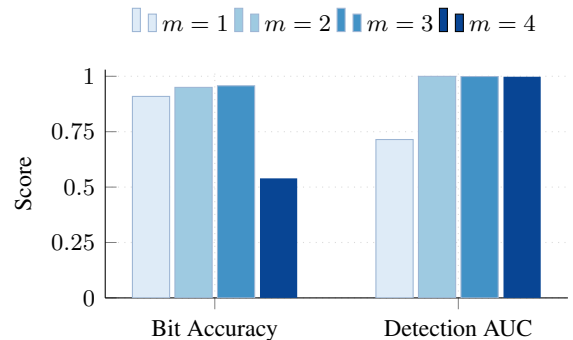


Figure 4: LFQA ablation of m for QuantileMark with 24 bits embedded. We vary the bits per symbol m ($M = 2^m$ quantile bins).

bol, explaining the drop in bit accuracy observed at $m = 4$.

The lower AUC at $m = 1$ stems from the sharp CDF geometry of human text. Human tokens often fall in the tail, yielding nearly deterministic bin posteriors. With binary partitions ($M = 2$), the detector’s maximization step can easily find a spurious message that fortuitously aligns with these strong signals. Increasing to $M = 4$ makes such chance agreement statistically much harder—as each token supports a specific bin while rejecting three others—thereby improving separation.

4.3 Robustness to Scrubbing Attacks on C4

We evaluate robustness on C4 under four scrubbing attacks commonly used in prior multi-bit wa-

Method	No attack		Copy-paste ($\epsilon = 0.2$)		Synonym ($\epsilon = 0.2$)		Deletion ($\epsilon = 0.1$)		Paraphrase (Dipper)	
	Bit Acc \uparrow	AUC \uparrow	Bit Acc \uparrow	AUC \uparrow	Bit Acc \uparrow	AUC \uparrow	Bit Acc \uparrow	AUC \uparrow	Bit Acc \uparrow	AUC \uparrow
MPAC	0.9702	0.9887	0.9438	0.9849	0.9476	0.9876	0.8811	0.9750	0.7201	0.7936
StealthInk	0.9003	0.9869	0.8497	0.9550	0.8608	0.9701	0.7839	0.8854	0.6829	0.6536
QuantileMark	0.9893	0.9995	0.9730	0.9972	0.9712	0.9963	0.8712	0.9426	0.7640	0.7609

Table 2: Robustness on C4 with 24 bits embedded in 300 tokens. The attack intensities ϵ denote the fraction of tokens modified.

Method	Machine translation			Summarization		
	BLEU \uparrow	R-1 \uparrow	BERTScore (BERT) \uparrow	R-1 \uparrow	BERTScore (BERT) \uparrow	PPL \downarrow
No watermark	17.55	49.13	35.82	37.42	21.40	5.18
MPAC	16.89	47.98	34.89	36.81	20.57	5.81
StealthInk	17.42	48.97	35.75	37.08	20.83	5.72
QuantileMark	17.41	48.99	35.99	37.44	21.37	5.21

Table 3: Downstream generation quality under top- $k=128$ sampling. For machine translation, we report BLEU, ROUGE-1 (R-1), and BERTScore (BERT). For summarization, we report ROUGE-1, BERTScore, and perplexity (PPL).

termark evaluations (Jiang et al., 2025): copy-paste mixing with non-watermarked text, synonym substitution, random deletion, and paraphrasing. Table 2 reports bit accuracy and detection AUC; full attack specifications are described in Appendix D.2.

While the watermark resists local lexical edits (copy-paste and substitution), deletions and paraphrasing prove significantly more damaging. These attacks induce synchronization drift and degrade the context quality required to reconstruct the quantile geometry, thereby hindering the recovery of long multi-bit messages. Robust detection under paraphrasing remains an open challenge across all existing multi-bit watermarking schemes.

4.4 Detector-Generator Mismatch on LFQA

We evaluate detector-generator mismatch when text is generated with ($k=128, \tau=1.0$) but detector varies ($\hat{k}, \hat{\tau}$). Figure 5 shows that performance degrades smoothly under moderate mismatch: bit accuracy remains high across $\hat{\tau} \in [0.8, 1.2]$ and remains stable even for small detector top- \hat{k} (e.g., $\hat{k} = 8$). This robustness is expected in our white-box setting because the detector reconstructs quantile geometry from logits: moderate changes in truncation or temperature often preserve the probability ordering on the head of the distribution, so overlap masses and channel posteriors shift gradually rather than catastrophically.

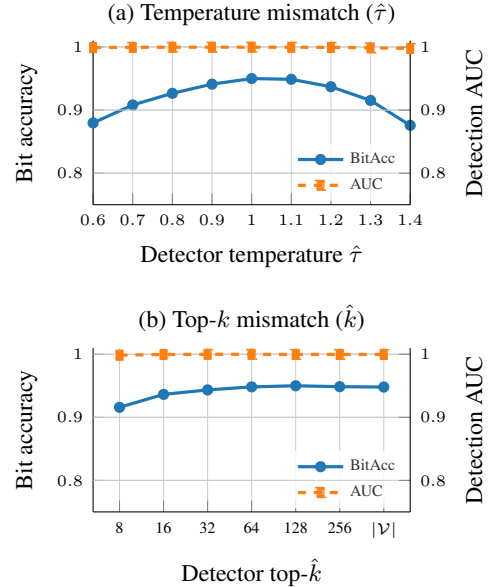


Figure 5: Detector-generator mismatch analysis on Llama-3.1-8B-Instruct.

4.5 Utility on Downstream Tasks

Finally, we assess whether watermarking degrades downstream utility under top- $k=128$ sampling. For text summarization, we use BART-large (Lewis et al., 2020) evaluated on CNN/DailyMail (Hermann et al., 2015). For machine translation, we run Multilingual BART (mBART) (Liu et al., 2020) on the WMT’14 En-Ro corpus (Bojar et al., 2014). We also include a reference-free LFQA evaluation using GPT-4o, with the full experimental setup and results detailed in Appendix E.2.

Table 3 shows that QuantileMark consistently outperforms other watermarking baselines, achieving utility scores that are nearly identical to the no-watermark upper bound across both tasks.

5 Related Work

We focus on generative watermarking schemes that modify the sampling process, distinguishing between distortionary partitioning and distribution-preserving methods.

5.1 Distortionary Vocabulary Partitioning Multi-bit Watermarks

A dominant line of work constructs a channel by partitioning the vocabulary and biasing the next token distribution toward a key dependent subset. The watermark of Kirchenbauer et al. (2023) introduces green list promotion with statistical tests on set hits, followed by analyses of calibration and robustness under edits (Piet et al., 2023; Kirchenbauer et al., 2024). Multi bit extensions retain the same mechanism while adding structure across positions, for example via position allocation and multiple colorings in MPAC (Yoo et al., 2024), or via coding designs over partition assignments (Wang et al., 2024; Fernandez et al., 2023). Several works improve robustness by adding error correcting codes from the view of message encoding (Chao et al., 2025; Qu et al., 2024).

However, standard partitioning schemes inherently suffer from probability mass imbalance, particularly in peaked distributions. While recent heuristics like rank-based partitioning (Park et al., 2025) or entropy-based gating (Gu et al., 2025) mitigate this issue, they remain adaptive approximations. In contrast, QuantileMark addresses this structurally by redefining channels in CDF interval, guaranteeing an equal probability budget by construction rather than adaptive rejection.

5.2 Distribution-preserving and Unbiased Watermarks

A parallel line of work aims to preserve the base model distribution in expectation over the watermark randomness. Two complementary perspectives predominate in the literature: *RNG-space* constructions, which define a measure-preserving transformation on the sampling randomness (Kuditipudi et al., 2024), and *reweighting* constructions, which formulate watermarking as a randomized modification of the stepwise token distribution (Hu et al., 2024).

RNG-space distortion-free watermarks. Kuditipudi et al. (2024) propose distortion-free watermarking by mapping a key-derived random number sequence to samples from the language model, and instantiate the framework with inverse transform sampling and exponential minimum sampling. SynthID-Text introduces Tournament sampling (Dathathri et al., 2024). Multi-bit extensions encode information by transforming the sampling randomness based on the message: DISC employs

cyclic shifts (Kordi Boroujeny et al., 2024), while MirrorMark utilizes measure-preserving mirroring (Anonymous, 2025).

Expectation-unbiased reweighting. Hu et al. (2024) formalize unbiased watermarking as randomized reweighting of the stepwise distribution. For autoregressive generation, preserving the sequence distribution requires appropriate independence of the watermark codes across steps (Hu et al., 2024). DiPmark (Wu et al., 2024) and StealthInk (Jiang et al., 2025) further explore distribution-preserving designs, with StealthInk emphasizing text-only detection and multi-bit provenance.

QuantileMark shares the design of defining watermarks through structured sampling randomness but leverages white-box access to optimize for detection reliability rather than black-box stealth. Unlike prior schemes that rely on randomized vocabulary partitions, QuantileMark enforces equal-mass channelization on the cumulative probability interval. This structural design substantially boosts the stepwise statistical evidence available for decoding, all while maintaining the theoretical unbiasedness of the generation process.

6 Conclusion

We presented **QuantileMark**, a white-box multi-bit watermark designed to mitigate the challenges of provenance embedding in low-entropy regimes. Instead of relying on vocabulary partitioning, QuantileMark defines the channel in cumulative probability interval by dividing it into M equal-mass bins. This structural approach ensures that every symbol receives a fixed probability budget, providing a basis for *message symmetry* where messages are treated with consistent statistical weight. Complementing this embedding, we derived a teacher-forced detector that exploits the reconstructed quantile geometry to compute posteriors over latent bins, enabling a coherent decode-then-test process. Empirical results across base and instruction-tuned models demonstrate the feasibility and effectiveness of this design, showing improved recovery rates and detection performance compared to vocabulary-based baselines—even under decoding parameter mismatch—while preserving generation quality. QuantileMark thus offers a practically viable solution for provider-internal attribution that balances structural consistency with operational utility.

597 Limitations

598 Our work has several limitations that suggest direc-
599 tions for future research. First, robustness remains
600 limited under heavy paraphrasing and other edits
601 that substantially rewrite local contexts, since such
602 changes can disrupt position allocation and the seed
603 stream used for per-step relabeling and evidence
604 aggregation. Improving paraphrase resilience may
605 require stronger position allocation strategies that
606 tolerate sequence misalignment and a PRF or seed-
607 ing logic that depends less on fragile local token
608 neighborhoods while remaining reproducible for
609 the key holder. Second, our study focused on a
610 provider-internal setting and assumed white-box
611 access at detection time, which rules out public
612 verification from text alone in the current form. Al-
613 though detection may transfer to settings with a
614 proxy model, a distilled model, or a closely related
615 model family sharing the same tokenizer, we did
616 not systematically study how model mismatch and
617 distribution shift affect the reconstructed geometry
618 and downstream recovery. Finally, our experimen-
619 tal evaluation was limited in scope, utilizing a small
620 set of tasks and model families. Extending eval-
621 uation across broader decoding policies settings
622 would better characterize the generality of quantile-
623 based channelization for multi-bit provenance.

624 References

625 Anonymous. 2025. MIRRORMARK: A distortion-
626 free multi-bit watermark for large language mod-
627 els. *OpenReview preprint*. ICLR 2026 submission,
628 available at [https://openreview.net/forum?id=](https://openreview.net/forum?id=3GNaNi9xnt)
629 [3GNaNi9xnt](https://openreview.net/forum?id=3GNaNi9xnt).

630 Ondrej Bojar, Christian Buck, Christian Federmann,
631 Barry Haddow, Philipp Koehn, Johannes Leveling,
632 Christof Monz, Pavel Pecina, Matt Post, Herve Saint-
633 Amand, Radu Soricut, Lucia Specia, and Ale s Tam-
634 chyna. 2014. *Findings of the 2014 workshop on*
635 *statistical machine translation*. In *Proceedings of the*
636 *Ninth Workshop on Statistical Machine Translation*,
637 pages 12–58, Baltimore, Maryland, USA. Associa-
638 tion for Computational Linguistics.

639 Patrick Chao, Yan Sun, Edgar Dobriban, and Hamed
640 Hassani. 2025. Watermarking language mod-
641 els with error correcting codes. *arXiv preprint*
642 *arXiv:2406.10281*.

643 Sumanth Dathathri, Abigail See, Sumedh Ghaisas, Po-
644 Sen Huang, Rob McAdam, Johannes Welbl, Van-
645 dana Bachani, Alex Kaskasoli, Robert Stanforth,
646 Tatiana Matejovicova, Jamie Hayes, Nidhi Vyas,
647 Majd Al Meray, Jonah Brown-Cohen, Rudy Bunel,
648 Borja Balle, A. Taylan Cemgil, Zahra Ahmed, Kitty

Stacpoole, and 5 others. 2024. *Scalable watermark-*
ing for identifying large language model outputs.
Nat., 634(8035):818–823.

Angela Fan, Yacine Jernite, Ethan Perez, David Grang-
ier, Jason Weston, and Michael Auli. 2019. *ELI5:*
long form question answering. In *Proceedings of*
the 57th Conference of the Association for Compu-
tational Linguistics, ACL 2019, Florence, Italy, July
28- August 2, 2019, Volume 1: Long Papers, pages
3558–3567. Association for Computational Linguis-
tics.

Pierre Fernandez, Antoine Chaffin, Karim Tit, Vivien
Chappelier, and Teddy Furon. 2023. Three bricks to
consolidate watermarks for large language models.
In *2023 IEEE International Workshop on Information*
Forensics and Security (WIFS). IEEE.

Aaron Grattafiori, Abhimanyu Dubey, Abhinav Jauhri,
Abhinav Pandey, Abhishek Kadian, Ahmad Al-
Dahle, Aiesha Letman, Akhil Mathur, Alan Schel-
ten, Alex Vaughan, Amy Yang, Angela Fan, Anirudh
Goyal, Anthony Hartshorn, Aobo Yang, Archi Mi-
tra, Archie Sravankumar, Artem Korenev, Arthur
Hinsvark, and 542 others. 2024. *The llama 3 herd of*
models. *Preprint*, arXiv:2407.21783.

Tianle Gu, Zongqi Wang, Kexin Huang, Yuanqi Yao,
Xiangliang Zhang, Yujiu Yang, and Xiuying Chen.
2025. *Invisible entropy: Towards safe and efficient*
low-entropy LLM watermarking. In *Proceedings of*
the 2025 Conference on Empirical Methods in Natu-
ral Language Processing, pages 6727–6744, Suzhou,
China. Association for Computational Linguistics.

Karl Moritz Hermann, Tomas Kocisky, Edward Grefen-
sette, Lasse Espeholt, Will Kay, Mustafa Suleyman,
and Phil Blunsom. 2015. Teaching machines to read
and comprehend. *Advances in neural information*
processing systems, 28.

Zhengmian Hu, Lichang Chen, Xidong Wu, Yihan Wu,
Hongyang Zhang, and Heng Huang. 2024. *Unbiased*
watermark for large language models. In *The Twelfth*
International Conference on Learning Representa-
tions.

Ya Jiang, Chuxiong Wu, Massieh Kordi Boroujeny,
Brian L. Mark, and Kai Zeng. 2025. Stealthink: A
multi-bit and stealthy watermark for large language
models. *arXiv preprint arXiv:2506.05502*.

John Kirchenbauer, Jonas Geiping, Yuxin Wen,
Jonathan Katz, Ian Miers, and Tom Goldstein. 2023.
A watermark for large language models. In *Proceed-*
ings of the 40th International Conference on Machine
Learning, volume 202 of *Proceedings of Machine*
Learning Research, pages 17061–17084. PMLR.

John Kirchenbauer, Jonas Geiping, Yuxin Wen, Manli
Shu, Khalid Saifullah, Kezhi Kong, Kasun Fernando,
Aniruddha Saha, Micah Goldblum, and Tom Gold-
stein. 2024. *On the reliability of watermarks for large*
language models. In *ICLR*.

705	Massieh Kordi Boroujeny, Ya Jiang, Kai Zeng, and Brian Mark. 2024. Multi-Bit Distortion-Free Watermarking for Large Language Models. <i>arXiv preprint arXiv:2402.16578</i> .	762
706		763
707		764
708		765
709	Kalpesh Krishna, Yixiao Song, Marzena Karpinska, John Wieting, and Mohit Iyyer. 2023. Paraphrasing evades detectors of ai-generated text, but retrieval is an effective defense. In <i>Proceedings of the 37th International Conference on Neural Information Processing Systems, NIPS '23</i> , Red Hook, NY, USA. Curran Associates Inc.	766
710		767
711		768
712		769
713		770
714		771
715		772
716	Rohith Kuditipudi, John Thickstun, Tatsunori Hashimoto, and Percy Liang. 2024. Robust distortion-free watermarks for language models. <i>Transactions on Machine Learning Research</i> .	773
717		774
718		775
719		776
720		777
721	Mike Lewis, Yinhan Liu, Naman Goyal, Marjan Ghazvininejad, Abdelrahman Mohamed, Omer Levy, Veselin Stoyanov, and Luke Zettlemoyer. 2020. Bart: Denoising sequence-to-sequence pre-training for natural language generation, translation, and comprehension. In <i>Proceedings of the 58th Annual Meeting of the Association for Computational Linguistics</i> , pages 7871–7880.	778
722		779
723		780
724		781
725		782
726		783
727		784
728	Yinhan Liu, Jiatao Gu, Naman Goyal, Xian Li, Sergey Edunov, Marjan Ghazvininejad, Mike Lewis, and Luke Zettlemoyer. 2020. Multilingual denoising pre-training for neural machine translation. <i>Transactions of the Association for Computational Linguistics</i> , 8.	785
729		786
730		787
731		788
732		789
733	OpenAI, :, Aaron Hurst, Adam Lerer, Adam P. Goucher, Adam Perelman, Aditya Ramesh, Aidan Clark, AJ Ostrow, Akila Welihinda, Alan Hayes, Alec Radford, Aleksander Mądry, Alex Baker-Whitcomb, Alex Beutel, Alex Borzunov, Alex Carney, Alex Chow, Alex Kirillov, and 401 others. 2024. Gpt-4o system card. <i>Preprint</i> , arXiv:2410.21276.	790
734		791
735		792
736		793
737		794
738		795
739		796
740	OpenAI. 2022. ChatGPT: Optimizing language models for dialogue. Website. https://openai.com/blog/chatgpt .	797
741		798
742		799
743	Shinwoo Park, Hyejin Park, Hyeseon Ahn, and Yo-Sub Han. 2025. Watermod: Modular token-rank partitioning for probability-balanced llm watermarking. <i>Preprint</i> , arXiv:2511.07863.	800
744		801
745		802
746		803
747	Julien Piet, Chawin Sitawarin, Vivian Fang, Norman Mu, and David Wagner. 2023. Mark my words: Analyzing and evaluating language model watermarks. <i>arXiv preprint arXiv:2312.00273</i> .	804
748		805
749		806
750		807
751	Wenjie Qu, Dong Yin, Zixin He, Wei Zou, Tianyang Tao, Jinyuan Jia, and Jiaheng Zhang. 2024. Provably Robust Multi-bit Watermarking for AI-generated Text via Error Correction Code. <i>arXiv preprint arXiv:2401.16820</i> .	808
752		
753		
754		
755		
756	Colin Raffel, Noam Shazeer, Adam Roberts, Katherine Lee, Sharan Narang, Michael Matena, Yanqi Zhou, Wei Li, and Peter J Liu. 2020. Exploring the limits of transfer learning with a unified text-to-text transformer. <i>Journal of machine learning research</i> , 21(140).	
757		
758		
759		
760		
761		
	Hugo Touvron, Louis Martin, Kevin Stone, Peter Albert, Amjad Almahairi, Yasmine Babaei, Nikolay Bashlykov, Soumya Batra, Prajjwal Bhargava, Shrutu Bhosale, and 1 others. 2023. Llama 2: Open foundation and fine-tuned chat models. <i>arXiv preprint arXiv:2307.09288</i> .	
	Lean Wang, Wenkai Yang, Deli Chen, Hao Zhou, Yankai Lin, Fandong Meng, Jie Zhou, and Xu Sun. 2024. Towards codable watermarking for injecting multi-bits information to LLMs. In <i>The Twelfth International Conference on Learning Representations</i> .	
	Yihan Wu, Zhengmian Hu, Hongyang Zhang, and Heng Huang. 2024. Dipmark: A stealthy, efficient and resilient watermark for large language models. In <i>Proceedings of the 41st International Conference on Machine Learning</i> .	
	Zhiguang Yang, Gejian Zhao, and Hanzhou Wu. 2025. Watermarking for large language models: A survey. <i>Mathematics</i> , 13(9):1420.	
	KiYoon Yoo, Wonhyuk Ahn, and Nojun Kwak. 2024. Advancing beyond identification: Multi-bit watermark for large language models. In <i>Proceedings of the 2024 Conference of the North American Chapter of the Association for Computational Linguistics: Human Language Technologies (Volume 1: Long Papers)</i> , pages 4031–4055, Mexico City, Mexico. Association for Computational Linguistics.	
	A Channel Geometry and Message-Unbiasedness	
	This appendix collects auxiliary results that complement Section 3.2–3.4. We reuse the stepwise channel geometry from the main text but switch to a context-level notation by dropping the step index. Fix a context h and its decoding distribution $p_0(\cdot h)$. Define the discrete CDF F_h , token CDF intervals $I_h(y)$, equal-width quantile bins $\{B_r\}_{r \in [M]}$, and overlap mass	
	$\mu_h(y, r) := I_h(y) \cap B_r $	
	exactly as in Section 3.2.	
	A.1 Basic Overlap Identities	
	Lemma 2 (Basic overlap identities). For every context h :	
	$\sum_{r=0}^{M-1} \mu_h(y, r) = I_h(y) = p_0(y h), \quad \forall y \in \mathcal{V},$	
	$\sum_{y \in \mathcal{V}} \mu_h(y, r) = B_r = \frac{1}{M}, \quad \forall r \in [M]. \quad (7)$	
	<i>Proof.</i> Equation (6) holds because $\{B_r\}_r$ partitions $[0, 1)$. Equation (7) holds because $\{I_h(y)\}_y$ partitions $[0, 1)$.	

809 A.2 Unbiasedness Notions: Message and 810 Cipher

811 We recall two notions introduced in the main text.
812 Message-unbiasedness is defined in Definition 1,
813 and cipher-unbiasedness (a StealthInk-style view-
814 point) is defined in Definition 2. In this appendix
815 we use a context-level notation by dropping the
816 step index: fix a context h and the correspond-
817 ing base distribution $p_0(\cdot | h)$. The overlap mass
818 $\mu_h(y, r)$ is defined exactly as in Section 3.2, and
819 the per-channel distribution satisfies

$$820 p_{\text{wm}}(y | h, r) = M \mu_h(y, r). \quad (8)$$

821 We now give the proof of Lemma 1, which is
822 stated in the main text.

823 *Proof of Lemma 1.* Fix h . By assumption, ϕ maps
824 a uniform symbol to a uniform bin, so $R = \phi(s)$ is
825 uniform on $[M]$ when s is uniform on $[M]$. There-
826 fore, for any token $y \in \mathcal{V}$,

$$827 \mathbb{E}_s[p_{\text{wm}}(y | h, R)] = \mathbb{E}_R[p_{\text{wm}}(y | h, R)] \\ 828 = \frac{1}{M} \sum_{r=0}^{M-1} p_{\text{wm}}(y | h, r) \\ 829 = \frac{1}{M} \sum_{r=0}^{M-1} M \mu_h(y, r) \\ 830 = \sum_{r=0}^{M-1} \mu_h(y, r) \\ 831 = p_0(y | h), \quad (9)$$

832 where the last equality uses (6).

833 **Lemma 3** (Uniform cipher-induced relabeling im-
834 plies cipher-unbiasedness). Fix (h, s) . Assume
835 that under the seed prior in Definition 2, the key-
836 derived permutation Φ induces $R = \Phi(s)$ that is
837 uniform on $[M]$. Then for every token $y \in \mathcal{V}$,

$$838 \mathbb{E}[p_{\text{wm}}(y | h, \Phi(s))] = p_0(y | h). \quad (10)$$

839 *Proof.* Under the assumption, R is uniform on $[M]$

even with s fixed. Hence

$$840 \mathbb{E}[p_{\text{wm}}(y | h, \Phi(s))] = \mathbb{E}_R[p_{\text{wm}}(y | h, R)] \\ 841 = \frac{1}{M} \sum_{r=0}^{M-1} p_{\text{wm}}(y | h, r) \\ 842 = \frac{1}{M} \sum_{r=0}^{M-1} M \mu_h(y, r) \\ 843 = \sum_{r=0}^{M-1} \mu_h(y, r) = p_0(y | h), \\ 844 \quad (11)$$

845 where the last step uses (6).

846 A.3 Signal Dilution and Information Capacity

847 This subsection analyzes a fundamental decod-
848 ing limitation: the information recoverable about
849 the bin index is capped by the token surprisal
850 $-\log_2 p_0(y | h)$, regardless of watermark capacity
851 m .

852 **Posterior Bound.** Fix a context h and observed
853 token y . Assuming a uniform prior $\mathbb{P}(R = r) =$
854 $1/M$, the posterior for bin r is given by Eq. (26):
855 $\mathbb{P}(R = r | y, h) = \mu_h(y, r)/p_0(y | h)$. Since the
856 overlap mass satisfies $\mu_h(y, r) \leq |B_r| = 1/M$, the
857 posterior is uniformly bounded:

$$858 \max_{r \in [M]} \mathbb{P}(R = r | y, h) \leq \min \left\{ 1, \frac{1}{M p_0(y | h)} \right\}. \quad (12)$$

859 Intuitively, if a token's probability mass p_0 spans
860 many bins ($M p_0 \gg 1$), the probability is diluted
861 across all contained bins, preventing confident iden-
862 tification of any single bin.

863 **Information Cap.** The information gain
864 $\Delta(y) := H(R) - H(R | y, h)$ is bounded by the
865 min-entropy. Using (12):

$$866 \Delta(y) \leq \min\{\log_2 M, -\log_2 p_0(y | h)\}. \quad (13)$$

867 This bound implies that high-probability tokens
868 cannot carry more bits of watermark information
869 than their own self-information. For instance, if
870 $p_0(y | h) \geq 0.5$, observing y yields at most 1 bit
871 of information about the bin location, regardless of
872 how large M is. Reliable multi-bit recovery there-
873 fore relies on aggregating partial evidence across
874 the sequence rather than identifying the bin from a
875 single step.

876 A.4 Time-Averaged Bin Occupancy under a 877 Fixed Message

878 This subsection models the empirical occupancy
879 of quantile bins along a long continuation. Fix a
880 message $s_{1:H} \in [M]^H$ and consider a length- T
881 generated continuation $x_{1:T}$. At step t , the embed-
882 ding rule selects a target bin index

$$883 r_t^* := \phi_t(s_{i_t}) \in [M],$$

884 where (i_t, ϕ_t) are derived from the key K and the
885 step seed (e.g., $z_t = \text{Hash}(g_t)$ as in the main text).
886 Define the empirical bin occupancy

$$887 \hat{\pi}_T(r) := \frac{1}{T} \sum_{t=1}^T \mathbf{1}\{r_t^* = r\}, \quad r \in [M]. \quad (14)$$

888 When $\hat{\pi}_T$ is close to uniform, the scheme exhibits
889 a channel-hopping effect over time: although each
890 step samples within a single bin, the visited bins
891 cover $[M]$ nearly evenly at the sequence level.

892 We formalize this effect under an idealized PRF
893 model, conditioning on the realized sequence of
894 step seeds. Let \mathcal{Z}_T be the set of distinct seeds
895 appearing among $\{z_t\}_{t=1}^T$. For each $z \in \mathcal{Z}_T$, define
896 its multiplicity

$$897 n_z := |\{t \in [T] : z_t = z\}|, \quad \sum_{z \in \mathcal{Z}_T} n_z = T. \quad (15)$$

898 Because PRF outputs are functions of z , repeated
899 seeds reuse the same (i_t, ϕ_t) . Thus, for each dis-
900 tinct seed z , define the induced bin label

$$901 R_z := \phi_z(s_{i_z}) \in [M],$$

902 where (i_z, ϕ_z) denotes the PRF-derived pair asso-
903 ciated with seed z . Abbreviate

$$904 S_T := \sum_{z \in \mathcal{Z}_T} n_z^2, \quad T_{\text{eff}} := \frac{T^2}{S_T}. \quad (16)$$

905 Here T_{eff} acts as an effective sample size: repeated
906 seeds inflate S_T and reduce concentration.

907 **Proposition 1** (Key-random occupancy is near-u-
908 niform, with an effective sample size). Assume
909 an idealized PRF model in which, conditional
910 on the realized seed sequence (z_1, \dots, z_T) , the
911 pairs $\{(i_z, \phi_z)\}_{z \in \mathcal{Z}_T}$ are independent across dis-
912 tinct seeds, and each ϕ_z is a uniform random per-
913 mutation on $[M]$ independent of i_z . Then for any
914 fixed message $s_{1:H}$ and any $r \in [M]$,

$$915 \mathbb{E}[\hat{\pi}_T(r) \mid (z_1, \dots, z_T)] = \frac{1}{M}. \quad (17)$$

Moreover, for any $\epsilon > 0$, let $\mathbf{z} := (z_1, \dots, z_T)$.

$$\mathbb{P}\left(\left|\hat{\pi}_T(r) - \frac{1}{M}\right| \geq \epsilon \mid \mathbf{z}\right) \leq 2 \exp\left(-\frac{2\epsilon^2 T^2}{S_T}\right) \\ = 2 \exp(-2\epsilon^2 T_{\text{eff}}). \quad (18)$$

Proof. Condition on (z_1, \dots, z_T) . Grouping re-
peated seeds rewrites (14) as a weighted sum over
distinct seeds:

$$\hat{\pi}_T(r) = \sum_{z \in \mathcal{Z}_T} \frac{n_z}{T} \mathbf{1}\{R_z = r\}. \quad (19)$$

Under the permutation assumption, for any fixed
symbol $d \in [M]$ the image $\phi_z(d)$ is uniform on
 $[M]$, so $R_z = \phi_z(s_{i_z})$ is uniform on $[M]$ and
 $\mathbb{E}[\mathbf{1}\{R_z = r\} \mid (z_1, \dots, z_T)] = 1/M$, prov-
ing (17).

For concentration, let $X_z := \mathbf{1}\{R_z = r\} \in$
 $\{0, 1\}$ and weights $w_z := n_z/T$. The variables
 $\{X_z\}_{z \in \mathcal{Z}_T}$ are independent and $w_z(X_z - \mathbb{E}X_z) \in$
 $[-w_z, w_z]$. Applying the standard weighted Ho-
effding inequality yields

$$\mathbb{P}\left(\left|\sum_{z \in \mathcal{Z}_T} w_z \left(X_z - \frac{1}{M}\right)\right| \geq \epsilon \mid \mathbf{z}\right) \\ \leq 2 \exp\left(-\frac{2\epsilon^2}{\sum_{z \in \mathcal{Z}_T} w_z^2}\right). \quad (20)$$

Substituting $\sum_z w_z^2 = \sum_z (n_z/T)^2 = S_T/T^2$
gives (18).

This proposition highlights a purely *key-driven*
channel-hopping effect. Even with a fixed message
 $s_{1:H}$, the target mapping r_t^* visits bins nearly uni-
formly over time. This uniform coverage is critical
for preventing *structural bias*, ensuring that a de-
terministic message does not continuously target a
small subset of bins, which would otherwise induce
a perceptible distributional shift.

Crucially, this uniformity ($\hat{\pi}_T(r) \approx 1/M$) de-
scribes the distribution of the *target labels*, not
necessarily the token statistics of unwatermarked
text. The PRF construction achieves a dual goal:
it generates a target distribution that is statistically
near-uniform (preventing the systematic overuse of
any single bin) while remaining fully determinis-
tic and reproducible for the key holder (enabling
decoding). Finally, the effective sample size T_{eff}

accounts for the redundancy caused by seed collisions: repeated seeds force the reuse of PRF outputs, thereby reducing the number of independent samples and slowing the convergence to uniformity.

B Detection as a Composite GLRT with LPO Evidence

This appendix formalizes the detection process as a Generalized Likelihood Ratio Test (GLRT) and justifies the use of Log Posterior Odds (LPO) as the stepwise evidence metric.

B.1 Hypotheses and the Composite Alternative

Let $x_{1:T}$ be an observed continuation and $h_t = x_{<t}$. We test

$$H_0 : x_{1:T} \sim p_0, \quad (21)$$

$$H_1 : x_{1:T} \sim p_{\text{wm}}(\cdot | s) \text{ for some message } s \in \mathcal{S}. \quad (22)$$

We assume the detector has white-box access to the model and can reconstruct $p_0(\cdot | h_t)$ via teacher forcing. All PRF-derived assignments are reproducible because they are derived per step from the secret key and a hash of a local context $g_t = x_{t-w:t-1}$ in the generated stream.

B.2 Sequence Likelihood under a Fixed Message

At each step, a message symbol determines a target channel index $r_t^* \in [M]$ (after relabeling), and the per-step watermarked distribution is $p_{\text{wm}}(x_t | h_t, s) = M \mu_{h_t}(x_t, r_t^*)$. Using the standard autoregressive factorization, we write

$$\begin{aligned} p_{\text{wm}}(x_{1:T} | s) &= \prod_{t=1}^T p_{\text{wm}}(x_t | h_t, s) \\ &= \prod_{t=1}^T M \mu_{h_t}(x_t, r_t^*), \quad (23) \\ p_0(x_{1:T}) &= \prod_{t=1}^T p_0(x_t | h_t). \end{aligned}$$

B.3 Decode-then-Test Equals a GLRT

The generalized likelihood ratio statistic for H_0 versus the composite alternative H_1 is

$$\Lambda_{\text{GLRT}}(x_{1:T}) := \frac{\max_{s \in \mathcal{S}} p_{\text{wm}}(x_{1:T} | s)}{p_0(x_{1:T})}. \quad (24)$$

Let $\hat{s} \in \arg \max_{s \in \mathcal{S}} \log p_{\text{wm}}(x_{1:T} | s)$ be the decoded message. Then the decode-then-test score

$$T_{\text{GLRT}}(x_{1:T}) := \log p_{\text{wm}}(x_{1:T} | \hat{s}) - \log p_0(x_{1:T}) \quad (25)$$

equals $\log \Lambda_{\text{GLRT}}(x_{1:T})$ up to tie-breaking.

B.4 Channel Posterior and Token Evidence

Introduce a latent channel variable $R_t \in [M]$ indicating which quantile bin generated token x_t . Given teacher-forced reconstruction of $p_0(\cdot | h_t)$ and the overlap geometry,

$$\mathbb{P}(R_t = r | x_t, h_t) = \frac{\mu_{h_t}(x_t, r)}{p_0(x_t | h_t)}. \quad (26)$$

We define per-token log-posterior odds (LPO) evidence for the channel event $R_t = r$:

$$\text{LPO}_t(r) := \log \frac{\mathbb{P}(R_t = r | x_t, h_t)}{1 - \mathbb{P}(R_t = r | x_t, h_t)}. \quad (27)$$

To avoid overloading watermark-level hypotheses, define the event-level hypotheses $G_1(r) : R_t = r$ and $G_0(r) : R_t \neq r$. Assume a uniform prior $\mathbb{P}(R_t = r) = 1/M$.

Lemma 4 (Token LPO as an event-level likelihood ratio up to a constant). Let the mixture under $G_0(r)$ be

$$p(x_t | G_0(r)) = \frac{1}{M-1} \sum_{j \neq r} p(x_t | R_t = j). \quad (28)$$

Then

$$\text{LPO}_t(r) = \log \frac{p(x_t | G_1(r))}{p(x_t | G_0(r))} - \log(M-1). \quad (28)$$

Proof. By Bayes' rule,

$$\begin{aligned} &\frac{\mathbb{P}(R_t = r | x_t, h_t)}{\mathbb{P}(R_t \neq r | x_t, h_t)} \\ &= \frac{p(x_t | R_t = r) \mathbb{P}(R_t = r)}{\sum_{j \neq r} p(x_t | R_t = j) \mathbb{P}(R_t = j)} \\ &= \frac{p(x_t | R_t = r)}{\sum_{j \neq r} p(x_t | R_t = j)} \\ &= \frac{1}{M-1} \cdot \frac{p(x_t | R_t = r)}{p(x_t | G_0(r))}. \end{aligned}$$

Taking logs yields the claim.

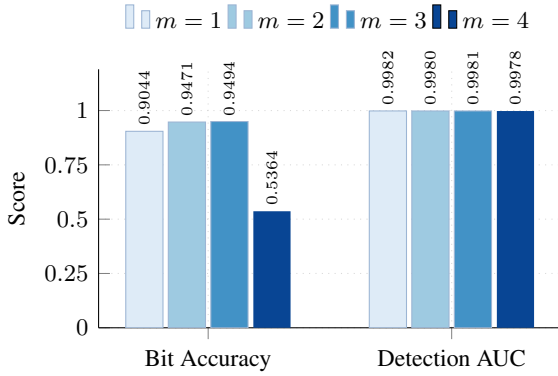


Figure 6: Performance comparison on LFQA with varying bits per symbol (m) using LLR as the token-level evidence. This serves as a complement to Figure 4, which uses LPO.

B.5 Comparison: LPO vs. LLR

For a fixed decoded message, the standard Log-Likelihood Ratio (LLR) evidence is:

$$\text{LLR}_t(r) := \log \frac{p_{\text{wm}}(x_t | h_t, r)}{p_0(x_t | h_t)} = \log M + \log p_t(r). \quad (29)$$

While LLR and LPO are functionally related via $\text{LPO}_t(r) = \text{LLR}_t(r) - \log M - \log(1 - p_t(r))$, LPO offers distinct numerical advantages.

Symmetry and Dynamic Range. We implement a clipped posterior $p_t(r) \in [\epsilon, 1 - \epsilon]$ (with $\epsilon = 10^{-6}$) for stability.

- **LLR** is asymmetric and capped from above: $\text{LLR}_t(r) \leq \log M$. Even if the token is perfectly aligned ($p_t(r) \approx 1$), the positive evidence is limited by the bit-width m .
- **LPO** is symmetric and unbounded (before clipping): $\text{LPO}_t \in [-C, C]$ where $C \approx 13.8$. This allows near-certain alignments to contribute significantly more evidence than $\log M$, improving separation when $p_t(r) \rightarrow 1$.

Empirical Validation. Table 4 and Figure 6 compare decoding using LPO versus LLR. While bit accuracy is similar (indicating decoding is driven by the rank order of posteriors), LPO yields higher detection AUC and better separation on C4.

C Relation to RNG Space and Reweighting Viewpoints

Section 5 surveys distribution preserving watermarking from the RNG space and reweighting

Evidence	Bit Acc \uparrow	Detection AUC \uparrow	Score on wm ($\mu \pm \sigma$)	Score on no wm ($\mu \pm \sigma$)
C4				
LPO	0.9868	0.9989	2.215 ± 1.134	-2.791 ± 0.531
LLR	0.9879	0.9751	-0.9069 ± 0.414	-3.336 ± 0.659
LFQA				
LPO	0.9500	0.9997	-0.046 ± 0.949	-3.152 ± 0.410
LLR	0.9470	0.9980	-0.899 ± 0.359	-4.291 ± 0.554

Table 4: Comparison of LPO and LLR evidence within QuantileMark ($m = 2, H = 12$) on C4 and LFQA. Score entries report mean \pm standard deviation.

viewpoints. This appendix clarifies how QuantileMark fits into the broader landscape of distribution-preserving watermarks, specifically comparing the handling of randomness and reweighting mechanisms.

C.1 RNG-Space Discretization and Unbiasedness

Standard distortion-free schemes typically define a measure-preserving map on the sampling randomness $u_t \in [0, 1)$, ensuring $x_t \sim p_0$ for every fixed message. In contrast, QuantileMark discretizes the RNG space $[0, 1)$ into M disjoint bins and restricts sampling to a specific bin B_{r^*} . Conceptually, this partitions the entropy source into a watermark-controlled variable (the bin index) and residual stochasticity (uniform sampling within the bin).

While this restriction implies the distribution is distorted for a *fixed* message, Lemma 1 proves that the scheme recovers p_0 when marginalized over the message or key. This design prioritizes **message symmetry** over strict per-message stealth. In provider-internal settings, this trade-off is advantageous: it maximizes the statistical evidence for detection while maintaining fairness and unbiasedness on average across the user base.

C.2 Vocabulary Shuffling versus CDF Message Relabeling

Some unbiased reweighting rules rely on shuffling a vocabulary order before applying accept amplify style operations (Hu et al., 2024; Jiang et al., 2025). QuantileMark does not require vocabulary shuffling. It keeps the CDF geometry fixed by the model induced probability ordering and uses only a low dimensional relabeling on $[M]$.

At each step, the PRF produces a message index assignment i_t and a permutation ϕ_t on $[M]$. The permutation relabels message symbols into

bin indices, and the bins themselves are defined by equal mass partitioning of the stepwise CDF. The randomized object is thus an element of $[M]$ or a permutation on $[M]$, rather than a randomized mask over \mathcal{V} . This keeps the embedding rule simple and makes reconstruction straightforward in a white box setting, since the detector can rebuild the same quantile geometry from logits and evaluate overlap masses directly.

D Detailed Experiment Setup

This appendix provides additional details on data preprocessing, filtering protocols, and the configuration of robustness attacks used in Section 4.

D.1 Dataset Details

C4 (Open-ended continuation). We utilize the realnewslike subset of the C4 dataset (Raffel et al., 2020). For each example, we truncate the first 50 tokens to serve as the prompt and treat the subsequent text as the human reference. To ensure valid comparisons, we first filter the dataset to retain only examples where the human reference exceeds the target evaluation length T .

LFQA (Long-form Question Answering). We use the ELI5/LFQA dataset (Fan et al., 2019), where the provided questions serve directly as prompts for the model. Similar to C4, we filter for human answers that exceed length T .

D.2 Attack Specifications

We evaluate robustness against four types of post-hoc editing attacks. For the first three attacks, the parameter ϵ controls the intensity of the distortion.

- **Copy-Paste Mixing:** This attack simulates a scenario where watermarked content is embedded within a larger non-watermarked context. We construct the attacked text by mixing a fraction $1 - \epsilon$ of the watermarked generation with a fraction ϵ of non-watermarked text. The watermarked segment is inserted contiguously to simulate a copy-paste operation.
- **Synonym Substitution:** We replace a fraction ϵ of the tokens in the watermarked text with their synonyms using a predefined synonym dictionary, while preserving the original sentence structure.
- **Random Deletion:** We randomly select and remove a fraction ϵ of tokens from the watermarked sequence.

Method	C4		LFQA	
	AUC \uparrow	TPR@1%FPR \uparrow	AUC \uparrow	TPR@1%FPR \uparrow
MPAC	0.9993	0.986	0.9744	0.8337
StealthInk	0.9851	0.6960	0.8081	0.1824
QuantileMark	0.9998	0.9900	0.9985	0.9499

Table 5: Detection performance on C4 and LFQA with 24 bits embedded in 300 tokens. Negatives are non-watermarked text generated by model.

- **Paraphrasing:** We employ DIPPER (Krishna et al., 2023), a paraphrase generation model designed for controlling lexical and syntactic diversity. Following standard evaluation protocols, we configure DIPPER with lexical diversity $L = 20$ and order diversity $O = 0$.

E Additional Results

E.1 Model Generation as Non-Watermarked Text

In the main text, we use human references as detection negatives (non-watermarked text) to reflect a deployment setting where provenance is verified among organic text. Since our detector is model-assisted and reconstructs token-level geometry via teacher forcing, the choice of negatives can interact with distribution mismatch between human text and the model. To isolate the watermark signal from such mismatch, we additionally evaluate detection where negatives are unwatermarked generations from the same base model, produced with the same prompts and decoding parameters as the watermarked texts. We report AUC and TPR at 1% FPR under this matched-model control, as Table 5 shows.

E.2 GPT-4o Judging for LFQA

We employ GPT-4o (OpenAI et al., 2024) as a reference-free judge for LFQA. The evaluator assesses the generated text directly and assigns a single integer score on a scale of 1 to 5. Following the protocol established by MirrorMark (Anonymous, 2025), we design the prompt to focus exclusively on linguistic quality while explicitly ignoring artifacts resulting from truncation. Table 6 shows the result.

rather than invasive profiling.

Method	GPT-4o \uparrow
No watermark	4.115
MPAC	3.921
StealthInk	4.047
QuantileMark	4.109

Table 6: LFQA answer quality judged by GPT-4o. Scores are on a 1–5 scale; higher is better. We randomly sample 500 prompts from LFQA and generate answers with a maximum length of $T=300$ new tokens. During evaluation, we exclude outputs shorter than 50 tokens to mitigate potential length-related bias.

GPT-4o Judge Prompt

You are a strict and consistent text-quality evaluator. Use ONLY the given text; do NOT assume the author’s intent. The text may start or end abruptly because the generation length is fixed. Do NOT penalize truncation or incompleteness. Do NOT judge factual correctness.

Rate each field as an integer from 1 to 5. **overall** is an independent judgment; do NOT compute overall from the other fields (no arithmetic).

Rate the following text. Return only a JSON object in exactly the following structure:

```
{
  "coherence": int,
  "clarity": int,
  "naturalness": int,
  "overall": int
}
```

Text: [TEXT]

F Potential Risks and Privacy Considerations

The primary ethical motivation for multi-bit watermarking is to enforce accountability, enabling the tracing of malicious outputs (e.g., disinformation) back to the responsible user. While this raises concerns regarding provider surveillance, we argue that the risk is mitigated by the passive nature of the system. The watermark serves as a silent signal that typically becomes actionable only when content is publicly disseminated by the user; in private settings, the signal remains inert. Furthermore, our provider-internal design offers superior privacy compared to black-box schemes where authorized verifiers might be granted decoding access. In our setting, the embedded identifier remains mathematically opaque to all external parties, ensuring that only the model host, the root of trust, can resolve identities. Ultimately, while the provider possesses the capability to link outputs to users, this power should be strictly governed by privacy policies and exercised solely for legitimate safety compliance